Blasticidin S inhibits translation by trapping deformed tRNA on the ribosome

Egor Svidritskiy[a], Clarence Ling[b], Dmitri N. Ermolenko[b,1], and Andrei A. Korostelev[a,1]

[a]RNA Therapeutics Institute, Department of Biochemistry and Molecular Pharmacology, University of Massachusetts Medical School, Worcester, MA 01605; and [b]Department of Biochemistry and Biophysics, Center for RNA Biology, School of Medicine and Dentistry, University of Rochester, Rochester, NY 14642

Edited by Jennifer A. Doudna, University of California, Berkeley, CA, and approved June 3, 2013 (received for review March 14, 2013)

The antibiotic blasticidin S (BlaS) is a potent inhibitor of protein synthesis in bacteria and eukaryotes. We have determined a 3.4-Å crystal structure of BlaS bound to a 70S·tRNA ribosome complex and performed biochemical and single-molecule FRET experiments to determine the mechanism of action of the antibiotic. We find that BlaS enhances tRNA binding to the P site of the large ribosomal subunit and slows down spontaneous intersubunit rotation in pretranslocation ribosomes. However, the antibiotic has negligible effect on elongation factor G catalyzed translocation of tRNA and mRNA. The crystal structure of the antibiotic–ribosome complex reveals that BlaS impedes protein synthesis through a unique mechanism by bending the 3′ terminus of the P-site tRNA toward the A site of the large ribosomal subunit. Biochemical experiments demonstrate that stabilization of the deformed conformation of the P-site tRNA by BlaS strongly inhibits peptidyl-tRNA hydrolysis by release factors and, to a lesser extent, peptide bond formation.

peptidyl transfer | ribosome crystal structure | termination inhibitor | translation inhibitor | translation termination

The growing problem of pathogen resistance to existing antibacterials prompts a search for alternative modes of inhibiting bacterial growth. The development of new drugs can be facilitated by understanding the mechanisms of action of known antibiotics (1). Because of its central role in cell metabolism, the ribosome is the target of numerous inhibitors that bind to various sites on the ribosome and interfere with different steps of protein synthesis. One of the predominant modes of action of ribosomal antibiotics is the inhibition of peptide bond formation. A majority of peptidyl-transferase inhibitors, including the widely used antibacterials chloramphenicol, linezolid, and the lincosamides lincomycin and clindamycin, bind to the A site of the large ribosomal subunit at the peptidyl-transferase center of the ribosome (2–4). By contrast, blasticidin S (BlaS) binds to the P site of the large subunit (5) and inhibits the peptidyl-transferase reaction through a distinct mechanism, which is still poorly understood.

BlaS, produced by some *Streptomyces* species, is a nucleoside analog consisting of a cytosine bonded to a pyranose ring and attached to an *N*-methyl-guanidine tail (Fig. 1*A*). BlaS has long been known to be a potent inhibitor of protein synthesis in bacteria and eukaryotes (6, 7). A crystal structure of the 50S subunit from *Haloarcula marismortui* bound to BlaS in the absence of tRNA revealed that BlaS occupies the P site of the large subunit (5). Two molecules of BlaS interact with the P loop and form base pairs with the universally conserved G2251 and G2252 of 23S ribosomal RNA (*Escherichia coli* 70S ribosome numbering is used throughout this article). These base pairing interactions closely mimic those of the two cytosine residues of the conserved CCA 3′ terminus of tRNA bound in the P site. Based on the finding that two molecules of BlaS mimic the cytosine residues of the CCA 3′ end of the P-site tRNA, BlaS was proposed to inhibit protein synthesis by competing with tRNA binding to the P site (5). However, early biochemical studies demonstrated that BlaS enhances P-site binding of aminoacyl-CACCA, which mimics the 3′ end of aminoacylated tRNA (8) and modestly inhibits the binding of aminoacyl-CACCA to the A site (8, 9). Moreover, BlaS competes with A-site binding antibiotics, such as sparsomycin (10) and puromycin (11). Mammalian cells resistant to BlaS were shown to be also resistant to sparsomycin and puromycin, further suggesting that the inhibitory mode of action of BlaS may involve the binding of the drug to the A site (12). Thus, the mechanism of BlaS action remains a conundrum: how can BlaS, whose binding site overlaps with that for P-site tRNA, stabilize the binding of the pentanucleotide mimic of the 3′ end of tRNA to the P site on the 50S subunit (8) and inhibit binding of tRNA analogs and antibiotics to the A site?

In this work, we elucidate the mechanism of BlaS action by X-ray crystallography, single-molecule Förster resonance energy transfer (smFRET) and biochemical assays. We show that BlaS inhibits protein synthesis through a unique mechanism by bending the CCA end of P-site tRNA toward the A site of the large subunit. Stabilization of this unusual, deformed conformation of P-site tRNA by BlaS results in inhibition of peptide bond formation and peptidyl–tRNA hydrolysis by release factors.

Results and Discussion

BlaS Stabilizes tRNA in the P Site of the Large Ribosomal Subunit. Early biochemical experiments showed that BlaS stabilizes binding of tRNA analogs to the 50S P site (8), which appears to conflict with crystallographic data showing that the binding sites of BlaS and the CCA end of P-site tRNA overlap (5). To reexamine the effect of BlaS on P-site binding, we used a filter-binding assay to monitor the binding of N-formyl-methionyl-tRNA^{fMet} (fMet-tRNA^{fMet}) to the P site of *E. coli* 70S ribosomes preincubated with various concentrations of BlaS in the presence of defined mRNA. Importantly, in contrast to previous biochemical experiments (8, 9), we used full-length initiator [^{35}S]-fMet-tRNA^{fMet} instead of short tRNA analogs, such as CACCA. No inhibition of tRNA binding was observed at concentrations of the antibiotic ≤1 mM (Fig. 1*B*). BlaS interfered with [^{35}S]-fMet-tRNA^{fMet} binding to the ribosome only at millimolar antibiotic concentrations (IC_{50} ~20 mM), i.e., concentrations that exceed the inhibition constant of BlaS for peptidyl transfer (200–400 nM; see 13, 14) by nearly five orders of magnitude. Notably, these concentrations exceed by up to four orders of magnitude the concentration of BlaS sufficient to abolish growth of bacterial and eukaryotic cells (7, 15–17). The destabilizing effect of large amounts of the antibiotic on tRNA binding is likely due to BlaS binding to a second, low-affinity site on the ribosome observed in the structure of the large ribosomal subunit from *H. marismortui* crystallized in the presence of 1–10 mM BlaS (5). In sum, the antibiotic does not hinder tRNA binding to the P site of the ribosome at concentrations that are inhibitory for protein synthesis and cell growth.

Author contributions: D.N.E. and A.A.K. designed research; E.S. and C.L. performed research; E.S., C.L., D.N.E., and A.A.K. analyzed data; and E.S., C.L., D.N.E., and A.A.K. wrote the paper.

The authors declare no conflict of interest.

This article is a PNAS Direct Submission.

Data deposition: The atomic coordinates and structure factors have been deposited in the Protein Data Bank, www.pdb.org (PDB ID codes 4L6J, 4L6K, 4L6L, and 4L6M).

[1]To whom correspondence may be addressed. E-mail: andrei.korostelev@umassmed.edu or Dmitri_Ermolenko@urmc.rochester.edu.

This article contains supporting information online at www.pnas.org/lookup/suppl/doi:10.1073/pnas.1304922110/-/DCSupplemental.

BIOCHEMISTRY

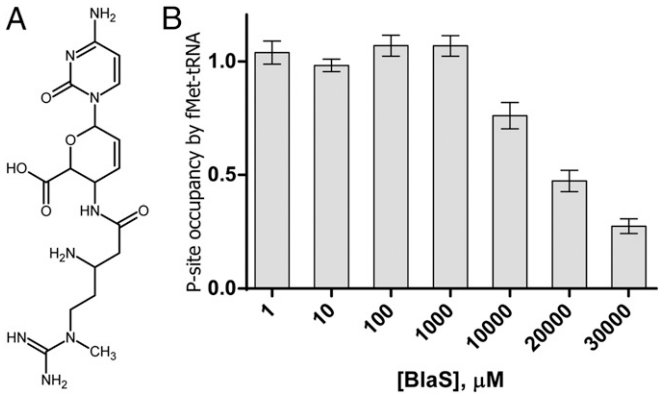

Fig. 1. Effect of BlaS on fMet-tRNA^{fMet} binding to the P site of the 70S ribosome. (*A*) Chemical structure of BlaS. (*B*) Binding of [^{35}S]-fMet-tRNA^{fMet} to the ribosome in the presence of mRNA and various concentrations of BlaS measured by a filter-binding assay. Bars show the P-site occupancy by [^{35}S]-fMet-tRNA^{fMet} relative to that in the ribosomes not treated with the antibiotic (the occupancy in the absence of the antibiotic is set to 1.0). Error bars show SDs calculated from triplicate measurements.

To further explore the effects of BlaS on tRNA affinity to the 50S P site, we asked whether BlaS affects the dynamics of ribosome-bound tRNAs, whose translocation through the ribosome is essential for protein synthesis. tRNA translocation, which is catalyzed by elongation factor G [EF-G (EF-2 in eukaryotes)], occurs in two steps. The acceptor ends of tRNAs first move relative to the large ribosomal subunit, from the classical A/A and P/P states into hybrid A/P and P/E states (Fig. 2*A*). The next step is the movement of anticodon stem loops of tRNAs on the small ribosomal subunit into posttranslocation P/P and E/E states. Whereas tRNA translocation on the small subunit requires EF-G and GTP, the movement of acceptor stems of peptidyl- and deacylated tRNAs on the large subunit occurs spontaneously, fluctuating between the classical (A/A and P/P) and hybrid (A/P and P/E) states (18–20). These spontaneous fluctuations of tRNAs are coupled to a rotation of the small ribosomal subunit relative to the large subunit between the nonrotated and rotated conformations, respectively (21–24). We previously developed a method to follow the intersubunit dynamics of the ribosome by measuring smFRET between fluorophores attached to protein S6 on the platform of the small ribosomal subunit and protein L9 on the large subunit (23). Using FRET in combination with total internal reflection microscopy, we have reported spontaneous fluctuations in single pretranslocation ribosomes between ~0.6 and ~0.4 FRET values, which correspond to the classical (nonrotated) and hybrid (rotated) states, respectively (22).

We examined how BlaS affects the affinity of tRNA to the 50S P site by monitoring the dynamics of single-tRNA fluctuations between the classical P/P and hybrid P/E states. To this end, we added tRNA^{Phe} to the P site of S6-Cy5/L9-Cy3-labeled ribosomes in the presence of defined mRNA and then flowed 1 mM BlaS into a sample cell. In the absence of BlaS, ribosomes underwent frequent intersubunit rotation and spent ~70% of the time in the rotated, hybrid-state conformation (Fig. 2*B*), consistent with prior observations (18–20). Addition of BlaS dramatically increased the fraction of nonrotated ribosomes, from ~30% to ~80% (Fig. 2*C* and Table S1). The rate of clockwise rotation of the 30S subunit coupled to tRNA transition from the hybrid P/E to the classical P/P state was unaffected by BlaS. By contrast, BlaS addition resulted in a fivefold reduction of the rate of counterclockwise rotation coupled with transition of tRNA from the classical P/P to the hybrid P/E state (Table S1). Ribosomes containing a single elongator tRNA^{Met} or initiator tRNA^{fMet} instead of tRNA^{Phe} behaved similarly (Fig. S1), underscoring that the effect of BlaS does not depend on tRNA identity. Inhibition of counterclockwise intersubunit rotation was recently observed in the presence of another peptidyl-transferase inhibitor, sparsomycin, which is also known to enhance tRNA binding to the 50S P site (25). We conclude that BlaS inhibits the transition of deacylated tRNA into the hybrid P/E state (Fig. 2*C*) via stabilization of the acceptor end of tRNA in the 50S P site, consistent with previous biochemical data (8, 9).

Effects of BlaS on the Dynamics of Pretranslocation Ribosomes and mRNA Translocation. We next tested the effect of BlaS on spontaneous intersubunit dynamics of authentic pretranslocation ribosomes containing tRNAs in both A and P sites (Fig. 2*A*). Similarly to ribosomes containing a single tRNA in the P site, the majority (~70%) of pretranslocation ribosomes containing the peptidyl-tRNA analog (18, 19, 26) *N*-acetyl-Phe-tRNA^{Phe} in the A site and deacylated elongator tRNA^{Met} in the P site adopt the rotated, hybrid-state conformation (Fig. 3*A*). In the presence of 1 mM BlaS, the majority of pretranslocation ribosomes (~60%) remained in the rotated state. This was surprising because BlaS dramatically shifted the distribution of ribosomes containing a single deacylated tRNA^{Met} toward the nonrotated, classical-state conformation (Fig. S1). However, kinetic analysis

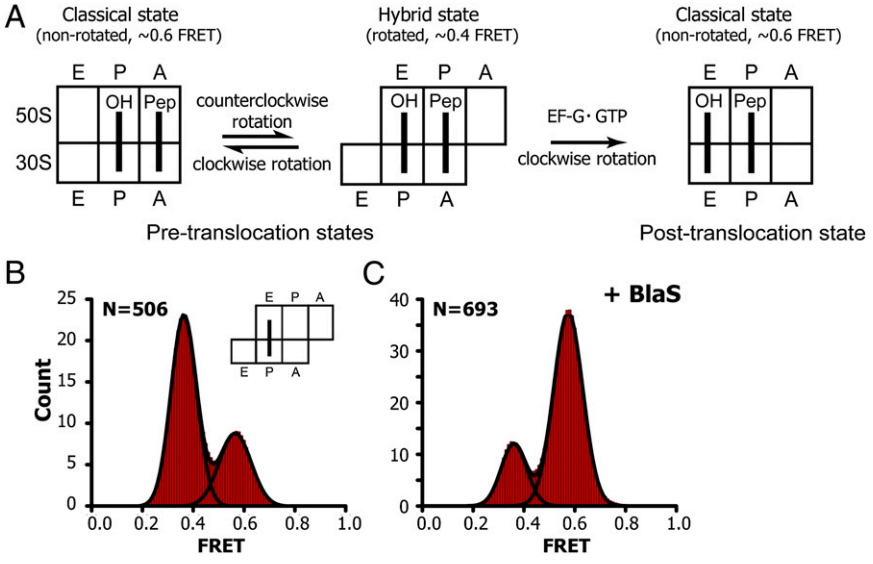

Fig. 2. Blasticidin S inhibits counterclockwise rotation of the 30S subunit coupled to the movement of deacylated tRNA into the hybrid P/E state. (*A*) Schematic depiction of intersubunit rotation, which is measured by smFRET, and tRNA movement during ribosomal translocation. (*B* and *C*) Histograms showing distributions of FRET values in ribosomes containing deacylated tRNA^{Phe} in the P site in the absence (*B*) or presence (*C*) of BlaS. N, number of single-molecule FRET traces compiled.

of single-molecule traces revealed that BlaS reduced the rates of both clockwise and counterclockwise rotation approximately sixfold, leaving the equilibrium constant (the ratio of rates for counterclockwise and clockwise intersubunit rotation) largely unaffected (Fig. S2 and Table S1). Inhibition of counterclockwise rotation of the 30S subunit coupled to transition of tRNA into hybrid states is likely due to stabilization of the acceptor end of deacylated tRNA in the 50S P site by BlaS, which fixes P-site tRNA in the P/P classical state (Fig. 2*A*). This echoes our observation for ribosomes containing a single deacylated tRNA in the P site (Fig. 2*B*). By contrast, inhibition of clockwise rotation of the 30S evidently occurs only in the presence of an A-site tRNA and is likely due to stabilization of the acceptor end of peptidyl-tRNA in the 50S P site by BlaS, which fixes A-site tRNA in the hybrid A/P state (Fig. 2*A*). Thus, in pretranslocation ribosomes containing tRNAs in both A and P sites, BlaS inhibits both the forward and reverse transitions between the classical and hybrid states of tRNA binding.

Because BlaS significantly slows down tRNA and intersubunit dynamics in pretranslocation ribosomes in the absence of EF-G, we next asked whether BlaS also inhibits EF-G-catalyzed translocation of mRNA and tRNA. EF-G·GTP transiently stabilizes the rotated, hybrid-state conformation (27) and induces translocation of the anticodon stem loops of tRNA and cognate codons of mRNA from A and P to P and E sites, respectively (26). Here, we followed the kinetics of mRNA translocation in the presence of EF-G·GTP and BlaS by measuring the fluorescence quenching of a fluorescein dye attached to the 3′ end of the mRNA as it moves within the ribosome (28). Pretranslocation ribosomes assembled with deacylated $tRNA^{Met}$ in the P site, *N*-acetyl-Phe-$tRNA^{Phe}$ in the A site, and fluorescein-labeled mRNA were mixed with EF-G·GTP in a stopped-flow apparatus. mRNA translocation was detected by rapid ($3.7 \pm 0.6\ s^{-1}$) quenching of the fluorescein dye (Fig. 3*C* and Table S2). When pretranslocation ribosomes were preincubated with BlaS, the apparent rate of translocation was only slightly reduced ($2.6 \pm 0.4\ s^{-1}$) (Fig. 3*C* and Table S2). Therefore, despite significant inhibition of spontaneous ribosome and tRNA dynamics by BlaS, EF-G-catalyzed translocation is almost unaffected by the presence of the antibiotic. Notably, perturbations of the P site of the large subunit by mutations in the P loop of 23S ribosomal RNA (G2252C and G2251C) were also shown to considerably affect the frequency of spontaneous tRNA fluctuations between classical and hybrid states (29) without dramatic effects on the rate of EF-G-induced translocation (30). Together, these observations suggest that formation of the hybrid state intermediate is accelerated by EF-G and is not a rate-limiting step of translocation.

The Crystal Structure of the 70S·tRNA Complex Bound with BlaS Reveals That BlaS Induces a Deformed Conformation of P-site tRNA. A previous crystal structure of BlaS bound to the vacant 50S subunit of the *H. marismortui* ribosome revealed that the binding site for two molecules of BlaS overlaps with the binding site for P-tRNA (5). How can the enhancement of tRNA binding to the 50S P site observed in our smFRET experiments be achieved by an antibiotic that appears to compete with tRNA? To resolve this paradox, we determined a 3.4 Å crystal structure of BlaS bound to the 70S *Thermus thermophilus* ribosome in the presence of deacylated $tRNA^{fMet}$ molecules in the P and E sites (Fig. 4*A* and Table S3). In previously reported structures of 70S elongation (31, 32) or termination (33–35) complexes, the overall conformations of deacylated initiator $tRNA^{fMet}$ are nearly identical to those of elongator tRNAs and peptidyl-tRNA analogs. Together with the finding that the action of BlaS is unlikely to depend on the identity of tRNA (Fig. S1), this suggests that our crystal structure reflects the structural mechanism of action of BlaS on initiating and elongating ribosomes.

Unlike in the crystal structure of the vacant 50S subunit bound with two molecules of BlaS, only one molecule is found in the 70S·tRNA complex (Fig. 4*B*). The conformation of BlaS is similar to that of molecule 1 in the 50S crystal structure (5); the all-atom rms difference between them is 0.57 Å, similar to the coordinate error at 3.4 Å resolution. The *N*-methyl-guanidine moiety of BlaS is stacked on the base of A2439 of 23S ribosomal RNA and is stabilized by interaction with the negatively charged pocket formed by the phosphate groups of A2439, A2600, and C2601 (Fig. 4*C*). A single binding site for BlaS next to G2251 agrees with chemical probing and mutational data. In particular, interaction of the *N*-methyl-guanidine tail of BlaS with A2439 explains protection of A2439 from chemical modification in the presence of BlaS (36, 37). Mutation of U2438 of 23S ribosomal RNA confers BlaS resistance in the archaeon *Halobacterium halobium* (38). This can be explained by disruption of the U2438:A2071 base pair, which likely results in displacement of the adjacent A2439 and disruption of the interaction between A2439 and BlaS.

In the 70S structure, BlaS forms a base pair with G2251 of the 23S ribosomal RNA and intercalates between C74 and A76 of the CCA end of P-site tRNA. This interaction replaces the base pairing between G2251 and C75 observed in antibiotic-free 70S·tRNA complexes (31, 32, 39), resulting in displacement of the acceptor arm and the CCA end of the P-tRNA toward the A site (Fig. 4*D*). The ribose-phosphate backbone of C75 is shifted by more than 7 Å, whereas those of the adjacent C74 and A76 are displaced by ~4 and ~2 Å, respectively. This large local rearrangement results in

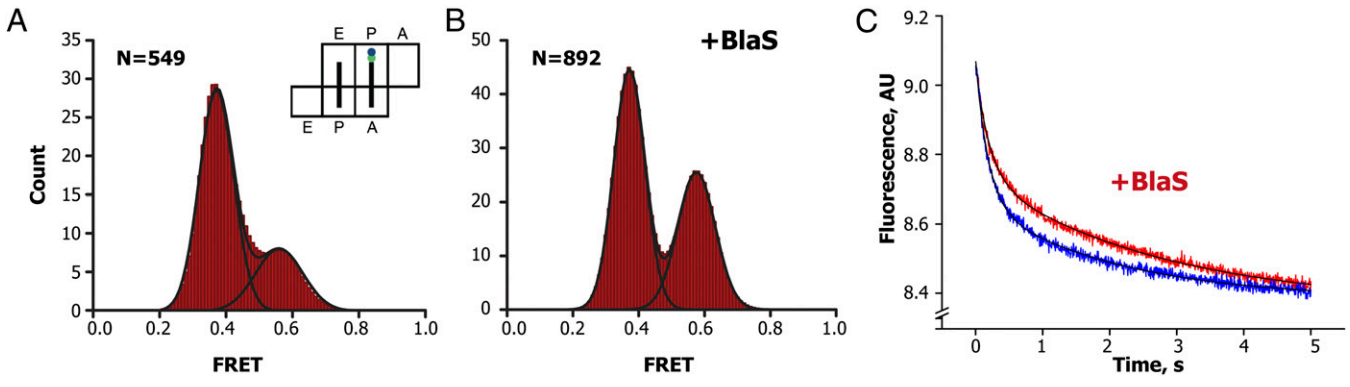

Fig. 3. Effects of BlaS on spontaneous intersubunit rotation in pretranslocation ribosomes and kinetics of EF-G-catalyzed mRNA translocation. (*A* and *B*) smFRET distribution histograms for pretranslocation ribosomes containing $tRNA^{Met}$ and *N*-acetyl-Phe-$tRNA^{Phe}$ in the P and A sites, respectively, in the absence (*A*) or presence (*B*) of BlaS. (*C*) Kinetics of EF-G-catalyzed translocation of mRNA in ribosomes preincubated with BlaS (red) or not treated with the antibiotic (blue). Kinetic measurements were performed in presteady-state stopped-flow kinetic experiments by the quenching of fluorescein attached to the mRNA. Pretranslocation ribosomes containing deacylated elongator $tRNA^{Met}$ in the P site and *N*-acetyl-Phe-$tRNA^{Phe}$ in the A site were mixed with GTP and EF-G. Double-exponential fits for fluorescein quenching are black curves.

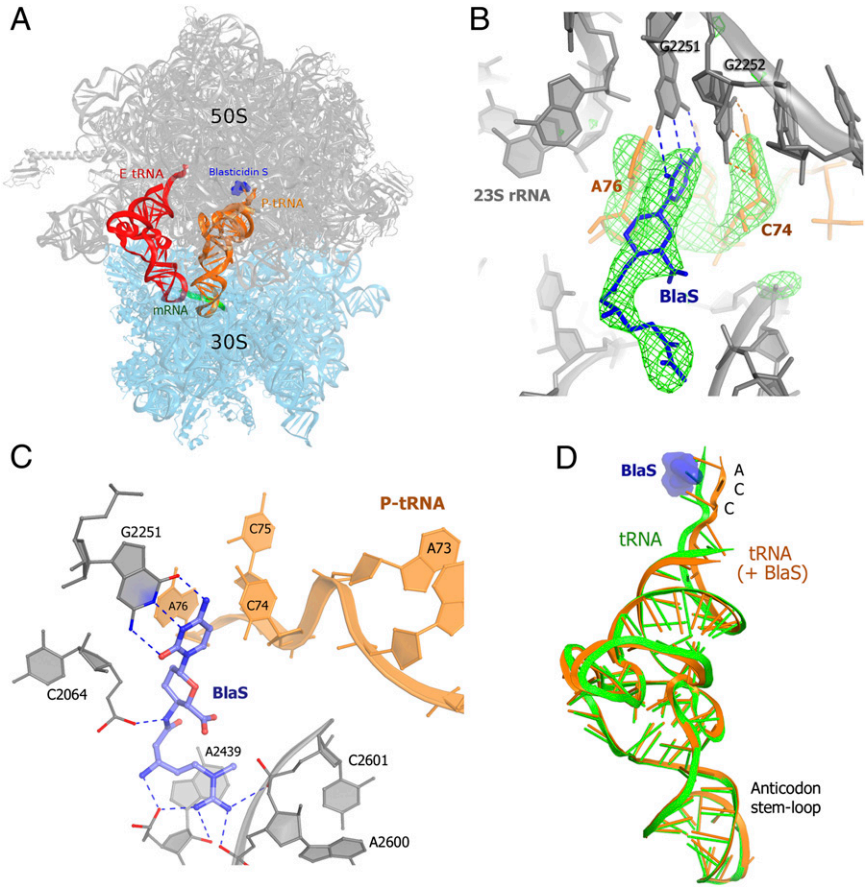

Fig. 4. Crystal structure of *T. thermophilus* 70S ribosome bound with BlaS in the presence of $tRNA^{fMet}$ in the P and E sites. (*A*) Positions of BlaS (blue), P-site (orange), and E-site (red) tRNAs; 30S subunit is in cyan and 50S subunit in gray. (*B*) Unbiased F_{obs}-F_{calc} density corresponding to BlaS and the CCA tail of the P-site tRNA. (*C*) Interactions of BlaS with the P site of the 50S subunit. (*D*) Superposition of tRNA in the 70S·tRNA·BlaS complex (orange, this work) with that from the antibiotic-free 70S·tRNA complex (green, ref. 31), demonstrating the BlaS-induced shift of the 3′ end toward the A site.

a ~4° rotation of the acceptor arm of the tRNA toward the 50S A site. The orientation of the rest of the P-site tRNA is nearly identical to that of the tRNA bound in the absence of BlaS (Fig. 4*D*). The movement of the CCA backbone caused by BlaS suggests that BlaS competition with A-site binding antibiotics (10, 11) is induced allosterically.

Whereas C74 is rearranged with respect to the 50S P site, it remains paired with G2252, whose base is moved by more than 1 Å codirectionally with the base of C74 (Fig. 4*B*). The ribose-phosphate backbone of the P loop is not affected by BlaS. The base of the terminal nucleotide A76, which is stacked on BlaS, remains in a position similar to that in the absence of BlaS (31, 32, 39). Intercalation of the cytosine moiety of BlaS between the bases of C74 and A76 likely compensates for the loss of stacking interaction of these nucleotides with C75. In addition, the 2′-hydroxyl group of C75 is positioned to hydrogen bond with the N4 position of the cytosine ring of the antibiotic, providing additional stabilization to the distorted conformation of tRNA. In sum, the stabilizing interactions that BlaS forms with ribosomal RNA and P-site tRNA explain the observed stabilization of the acceptor arm in the P site (Fig. 2*B*).

Our crystal structure provides insights into the mechanism of inhibition of peptidyl transfer by BlaS. Although the adenine moiety of A76 of the P-site tRNA is positioned to form an A-minor interaction with the A2450–C2063 bp of 23S ribosomal RNA (as in antibiotic-free complexes; see refs. 31, 32, 39), rearrangement of the CCA backbone results in detachment of the ribose of A76 from C2063. Rearrangement of the ribose moiety of A76 may result in suboptimal positioning of the peptidyl-tRNA and aminoacyl-tRNA substrates for nucleophilic attack, leading to inhibition of peptidyl transfer by BlaS.

BlaS Strongly Inhibits Peptide Release Mediated by RF1. The nucleophilic substitution reaction of peptide-bond formation is mechanistically similar to peptidyl-tRNA hydrolysis mediated by release factors 1 and 2 (RF1 and RF2), which bind to the ribosomal A site in response to stop codons and catalyze peptidyl-tRNA hydrolysis (40–43). Release factors are directly involved in peptidyl-tRNA hydrolysis by providing a catalytic group located in the universally conserved GGQ motif (40–43). We reasoned that in addition to its peptidyl-transfer inhibitory activity, BlaS may be a translation termination inhibitor. Superimposition of the BlaS-bound 70S structure with structures of 70S termination complexes (34, 35, 44) revealed that the distorted CCA end of the P-site tRNA in the BlaS-bound ribosomal complex substantially overlaps with the binding site for the GGQ-containing region of domain 3 of the release factors (Fig. 5*A*). This suggests that distortion of the P-site tRNA by BlaS may interfere with binding of release factors to the ribosome and/or prevent proper positioning of the GGQ motif for peptidyl-tRNA hydrolysis.

To test our hypothesis, we monitored the effect of BlaS on RF1-mediated peptide release from 70S ribosomes. We found that BlaS dramatically inhibits RF1-mediated [^{35}S]-fMet release from [^{35}S]-fMet-$tRNA^{fMet}$ bound to the P site of the ribosome in the presence of mRNA containing a UAA stop codon adjacent to an AUG codon. Specifically, BlaS nearly abolishes RF1-mediated release (Fig. 6*A*) at concentrations that were only modestly inhibitory to peptidyl transfer of [^{35}S]-fMet to puromycin (Fig. 6*B*), which is an A-site antibiotic that mimics the 3′ end of an aminoacyl-tRNA. The apparent inhibition constant (K_i) of 182 ± 39 nM for BlaS-dependent inhibition of the puromycin reaction determined from our measurements is consistent with previous estimates of a K_i between 200 nM (13) and 380 nM (14). Remarkably, the apparent K_i for the RF1-mediated release (32 ± 18 nM) is almost one order of magnitude lower than the K_i for the puromycin reaction. It is noteworthy that the sensitivity of the termination assay does not permit

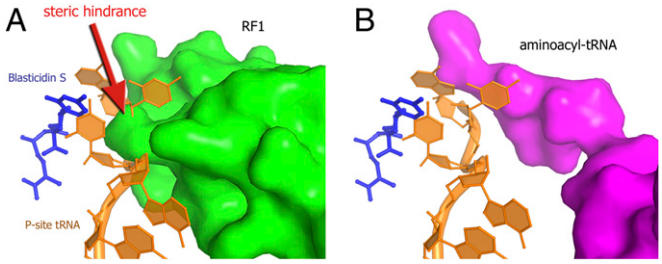

Fig. 5. Superposition of the 70S·BlaS structure (this work) with structures of 70S complexes whose A site is occupied by RF1 (35) or aminoacyl-tRNA analog (32). The superposition demonstrates that steric hindrance in the presence of BlaS is more pronounced in the case of release factor (*A*, green) than in the case of aminoacyl-tRNA (*B*, magenta).

measurements of peptide release at concentrations of the pretermination complex below 30 nM. Thus, the actual K_i for BlaS inhibition of termination may be even lower than the apparent K_i (~32 nM) determined from our experiments. Hence, our biochemical experiments demonstrate that BlaS is a more efficient inhibitor of translation termination than of peptidyl transfer (Fig. 6 *C* and *D*).

Conclusions

Our findings demonstrate that BlaS inhibits translation via a unique molecular mechanism that has not been previously documented for any antibiotic. The crystal structure of the BlaS-bound 70S ribosome complex reveals that unlike most peptidyl-transfer inhibitors, which bind in the vicinity of the A site of the 50S subunit, BlaS binds to the P site of the 50S subunit and bends the CCA end of the P-site tRNA toward the A site. The dramatic (>7 Å) shift of the ribose-phosphate backbone of C75 of the P-site tRNA underscores the conformational flexibility of tRNA. This observation expands our knowledge about the conformational space that tRNAs can sample during translation. More importantly, the distortion of the P-site tRNA explains the puzzling, previously reported ability of BlaS to interfere with binding of ribosomal ligands to the A site (8–11).

Our smFRET measurements show that BlaS slows down the intersubunit rotation in pretranslocation ribosomes that is coupled to spontaneous movement of tRNAs on the large subunit (Fig. 3*A*). This observation is consistent with early biochemical data demonstrating that BlaS increases tRNA affinity toward the 50S P site (8). Despite the inhibitory effect on tRNA fluctuations in a pretranslocation complex, EF-G-catalyzed translocation is affected only modestly (Fig. 3*B*). Our data therefore rule out the possibility that inhibition of translocation is a mode of BlaS action in vivo. Instead, our biochemical experiments suggest that BlaS may specifically target the termination step of protein synthesis.

We found that BlaS efficiently inhibits peptide release mediated by release factor RF1 during termination of protein synthesis and, to a lesser extent, peptidyl transfer during translation elongation. Inhibition of these steps of translation likely originates from a combination of two effects. First, the shift of the distorted CCA end of the P-site tRNA may occlude access of aminoacyl-tRNA and release factors into the A site on the 50S subunit (Figs. 4 and 5). The stronger inhibition of RF1-mediated peptide release by BlaS may result from a more pronounced steric interference of the distorted CCA end with the GGQ-containing region of release factors than with the A-site aminoacyl-tRNA (Fig. 5). Second, the terminal adenosine residue of the P-site tRNA is shifted from the position it occupies in the absence of the antibiotic (Fig. 4*D*). This rearrangement likely results in poor positioning of the peptidyl-tRNA substrate for nucleophilic attack by aminoacyl-tRNA during peptidyl transfer or by a water molecule during translation termination.

The strong inhibition of the translation termination step by BlaS is noteworthy because no specific inhibitors of translation termination have been identified so far (2, 45–47). Some inhibitors of peptide bond formation have been shown to also inhibit peptide release (2), but none has been quantitatively demonstrated to inhibit the latter step to a greater degree than peptidyl transfer (48). A large number of inherited and acquired diseases are attributed to the occurrence of a premature termination codon within the normal open reading frame, which precludes synthesis of full-length protein (49, 50). Because BlaS predominantly targets peptide release and also inhibits protein synthesis in eukaryotes (15, 17), our findings may potentially serve as a platform for the development of therapeutics that

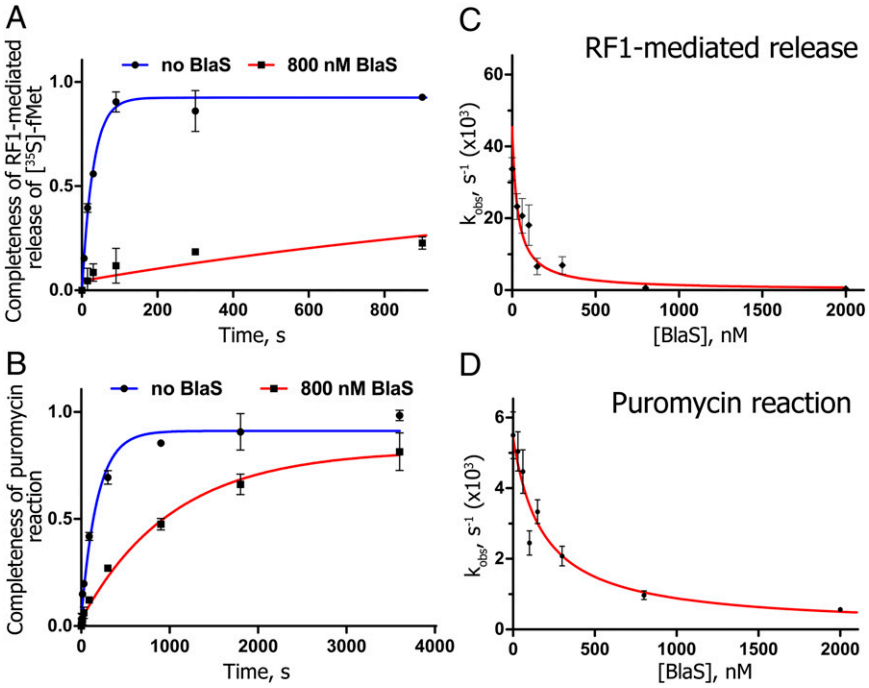

Fig. 6. BlaS is a potent inhibitor of RF1-mediated peptide release. (*A* and *B*) Time progress curves for RF1-mediated release (*A*) and peptidyl transfer to puromycin (*B*), respectively, in the absence (blue) or presence (red) of 800 nM BlaS. Pretermination complex was formed by incubating ribosomes with [^{35}S]-fMet-tRNA^{fMet} and mRNA containing the UAA termination codon next to the AUG codon. Then, pretermination ribosomes were incubated with either RF1 (*A*) or puromycin (*B*) and amounts of [^{35}S]-labeled release product were determined at several time points. Error bars represent SDs obtained from duplicate experiments. (*C* and *D*) Dependence of catalytic rates (k_{obs}) for RF1-mediated release (*C*) and puromycin reaction (*D*) on BlaS concentration. K_i for the peptide release and puromycin reaction was determined by hyperbola fitting (red) of k_{obs} values obtained at different concentrations of BlaS. Error bars represent residuals of single-exponential fitting of k_{obs} values to time progress curves.

specifically suppress translation termination in human diseases associated with premature termination codons.

Materials and Methods

Materials and methods are described in detail in *SI Materials and Methods*. Ribosomes, aminoacylated tRNAs, EF-G, and RF1 were prepared as previously described (23, 34, 44). Single-molecule FRET measurements were taken using a prism-type total internal reflection (TIR) microscope (22). Structure determination was performed using molecular replacement and yielded a structure with R/R^{free} of 0.232/0.268.

ACKNOWLEDGMENTS. We thank Rohini Madireddy for assistance with purification of RF1 and 70S ribosomes; staff members of beam lines 23ID-B and 23ID-D (Advanced Photon Source at Argonne National Laboratory) and X25 (National Synchrotron Light Source at Brookhaven National Laboratory, US Department of Energy, under Contract No. DE-AC02-98CH10886) for assistance with X-ray data collection; Jillian Dann and Enea Salsi for assistance with purification of ΔS6 and ΔL9 ribosomes and smFRET experiments, respectively; Peter Cornish for sharing MatLab scripts and advice on total internal reflection microscopy; Alexei V. Korennykh for stimulating discussions; and Harry F. Noller for comments on the manuscript. The study was supported by US National Institute of Health Grant GM-099719 (to D. N.E.) and Grant P30 GM092424 (to the Center for RNA Biology at University of Rochester). A.A.K. was supported by the Worcester Foundation for Biomedical Research and University of Massachusetts Medical School Center for AIDS Research.

1. Wimberly BT (2009) The use of ribosomal crystal structures in antibiotic drug design. *Curr Opin Investig Drugs* 10(8):750–765.
2. Wilson DN (2011) On the specificity of antibiotics targeting the large ribosomal subunit. *Ann N Y Acad Sci* 1241:1–16.
3. Yonath A (2005) Antibiotics targeting ribosomes: Resistance, selectivity, synergism and cellular regulation. *Annu Rev Biochem* 74:649–679.
4. Blaha GM, Polikanov YS, Steitz TA (2012) Elements of ribosomal drug resistance and specificity. *Curr Opin Struct Biol* 22(6):750–758.
5. Hansen JL, Moore PB, Steitz TA (2003) Structures of five antibiotics bound at the peptidyl transferase center of the large ribosomal subunit. *J Mol Biol* 330(5): 1061–1075.
6. Yamaguchi H, Tanaka N (1966) Inhibition of protein synthesis by blasticidin S. II. Studies on the site of action in E. coli polypeptide synthesizing systems. *J Biochem* 60(6):632–642.
7. Yamaguchi H, Yamamoto C, Tanaka N (1965) Inhibition of protein synthesis by blasticidin S. I. Studies with cell-free systems from bacterial and mammalian cells. *J Biochem* 57(5):667–677.
8. Cerná J, Rychlík I, Lichtenthaler FW (1973) The effect of the aminoacyl-4-aminohexosyl-cytosine group of antibiotics on ribosomal peptidyl transferase. *FEBS Lett* 30(2):147–150.
9. Pestka S (1974) The use of inhibitors in studies on protein synthesis. *Methods Enzymol* 30:261–282.
10. Lazaro E, van den Broek LA, San Felix A, Ottenheijm HC, Ballesta JP (1991) Biochemical and kinetic characteristics of the interaction of the antitumor antibiotic sparsomycin with prokaryotic and eukaryotic ribosomes. *Biochemistry* 30(40): 9642–9648.
11. Kalpaxis DL, Theocharis DA, Coutsogeorgopoulos C (1986) Kinetic studies on ribosomal peptidyltransferase. The behaviour of the inhibitor blasticidin S. *Eur J Biochem* 154(2):267–271.
12. Kuwano M, Takenaka K, Ono M (1979) The cross-resistance of mouse blasticidin S-resistant cell lines to puromycin and sparsomycin, inhibitors of ribosome function. *Biochim Biophys Acta* 563(2):479–489.
13. Theocharis DA, Synetos D, Kalpaxis DL, Drainas D, Coutsogeorgopoulos C (1992) Kinetics of inhibition of peptide bond formation on bacterial ribosomes. *Arch Biochem Biophys* 292(1):266–272.
14. Petropoulos AD, Xaplanteri MA, Dinos GP, Wilson DN, Kalpaxis DL (2004) Polyamines affect diversely the antibiotic potency: insight gained from kinetic studies of the blasticidin S AND spiramycin interactions with functional ribosomes. *J Biol Chem* 279(25):26518–26525.
15. Fukunaga K, Misato T, Ishii I, Asakawa M (1955) Blasticidin, a new anti-phytopathogenic fungal substance. Part I. *Bull Agric Chem Soc Jpn* 19:181–188.
16. Izumi M, et al. (1991) Blasticidin S-resistance gene (bsr): A novel selectable marker for mammalian cells. *Exp Cell Res* 197(2):229–233.
17. Takeuchi S, Hirayama K, Ueda K, Sakai H, Yonehara H (1958) Blasticidin S, a new antibiotic. *J Antibiot (Tokyo)* 11(1):1–5.
18. Blanchard SC, Kim HD, Gonzalez RL, Jr., Puglisi JD, Chu S (2004) tRNA dynamics on the ribosome during translation. *Proc Natl Acad Sci USA* 101(35):12893–12898.
19. Fei J, Kosuri P, MacDougall DD, Gonzalez RL, Jr. (2008) Coupling of ribosomal L1 stalk and tRNA dynamics during translation elongation. *Mol Cell* 30(3):348–359.
20. Munro JB, Altman RB, O'Connor N, Blanchard SC (2007) Identification of two distinct hybrid state intermediates on the ribosome. *Mol Cell* 25(4):505–517.
21. Agirrezabala X, et al. (2008) Visualization of the hybrid state of tRNA binding promoted by spontaneous ratcheting of the ribosome. *Mol Cell* 32(2):190–197.
22. Cornish PV, Ermolenko DN, Noller HF, Ha T (2008) Spontaneous intersubunit rotation in single ribosomes. *Mol Cell* 30(5):578–588.
23. Ermolenko DN, et al. (2007) Observation of intersubunit movement of the ribosome in solution using FRET. *J Mol Biol* 370(3):530–540.
24. Julián P, et al. (2008) Structure of ratcheted ribosomes with tRNAs in hybrid states. *Proc Natl Acad Sci USA* 105(44):16924–16927.
25. Ermolenko DN, Cornish PV, Ha T, Noller HF (2013) Antibiotics that bind to the A site of the large ribosomal subunit can induce mRNA translocation. *RNA* 19(2):158–166.
26. Ermolenko DN, Noller HF (2011) mRNA translocation occurs during the second step of ribosomal intersubunit rotation. *Nat Struct Mol Biol* 18(4):457–462.
27. Spiegel PC, Ermolenko DN, Noller HF (2007) Elongation factor G stabilizes the hybrid-state conformation of the 70S ribosome. *RNA* 13(9):1473–1482.
28. Studer SM, Feinberg JS, Joseph S (2003) Rapid kinetic analysis of EF-G-dependent mRNA translocation in the ribosome. *J Mol Biol* 327(2):369–381.
29. Wang L, Altman RB, Blanchard SC (2011) Insights into the molecular determinants of EF-G catalyzed translocation. *RNA* 17(12):2189–2200.
30. Dorner S, Brunelle JL, Sharma D, Green R (2006) The hybrid state of tRNA binding is an authentic translation elongation intermediate. *Nat Struct Mol Biol* 13(3):234–241.
31. Selmer M, et al. (2006) Structure of the 70S ribosome complexed with mRNA and tRNA. *Science* 313(5795):1935–1942.
32. Voorhees RM, Weixlbaumer A, Loakes D, Kelley AC, Ramakrishnan V (2009) Insights into substrate stabilization from snapshots of the peptidyl transferase center of the intact 70S ribosome. *Nat Struct Mol Biol* 16(5):528–533.
33. Weixlbaumer A, et al. (2008) Insights into translational termination from the structure of RF2 bound to the ribosome. *Science* 322(5903):953–956.
34. Korostelev A, et al. (2008) Crystal structure of a translation termination complex formed with release factor RF2. *Proc Natl Acad Sci USA* 105(50):19684–19689.
35. Laurberg M, et al. (2008) Structural basis for translation termination on the 70S ribosome. *Nature* 454(7206):852–857.
36. Rodriguez-Fonseca C, Amils R, Garrett RA (1995) Fine structure of the peptidyl transferase centre on 23 S-like rRNAs deduced from chemical probing of antibiotic-ribosome complexes. *J Mol Biol* 247(2):224–235.
37. Lichtenthaler FW, Trummlitz G (1974) Structural basis for inhibition of protein synthesis by the aminoacyl-aminohexosyl-cytosine group of antibiotics. *FEBS Lett* 38(3): 327–342.
38. Porse BT, Rodriguez-Fonseca C, Leviev I, Garrett RA (1995) Antibiotic inhibition of the movement of tRNA substrates through a peptidyl transferase cavity. *Biochem Cell Biol* 73(11-12):877–885.
39. Korostelev A, Trakhanov S, Laurberg M, Noller HF (2006) Crystal structure of a 70S ribosome-tRNA complex reveals functional interactions and rearrangements. *Cell* 126(6):1065–1077.
40. Zhou J, Korostelev A, Lancaster L, Noller HF (2012) Crystal structures of 70S ribosomes bound to release factors RF1, RF2 and RF3. *Curr Opin Struct Biol* 22(6):733–742.
41. Korostelev AA (2011) Structural aspects of translation termination on the ribosome. *RNA* 17(8):1409–1421.
42. Loh PG, Song H (2010) Structural and mechanistic insights into translation termination. *Curr Opin Struct Biol* 20(1):98–103.
43. Kisselev L, Ehrenberg M, Frolova L (2003) Termination of translation: Interplay of mRNA, rRNAs and release factors? *EMBO J* 22(2):175–182.
44. Korostelev A, Zhu J, Asahara H, Noller HF (2010) Recognition of the amber UAG stop codon by release factor RF1. *EMBO J* 29(15):2577–2585.
45. Nierhaus KH, Wilson DN (2004) *Protein Synthesis and Ribosome Structure* (Wiley-VCH, Weinheim).
46. Polacek N, et al. (2003) The critical role of the universally conserved A2602 of 23S ribosomal RNA in the release of the nascent peptide during translation termination. *Mol Cell* 11(1):103–112.
47. Caskey CT, Beaudet AL, Scolnick EM, Rosman M (1971) Hydrolysis of fMet-tRNA by peptidyl transferase. *Proc Natl Acad Sci USA* 68(12):3163–3167.
48. Kuzmiak HA, Maquat LE (2006) Applying nonsense-mediated mRNA decay research to the clinic: progress and challenges. *Trends Mol Med* 12(7):306–316.
49. Keeling KM, Bedwell DM (2011) Suppression of nonsense mutations as a therapeutic approach to treat genetic diseases. *Wiley Interdiscip Rev RNA* 2(6):837–852.
50. Peltz SW, Morsy M, Welch EM, Jacobson A (2013) Ataluren as an agent for therapeutic nonsense suppression. *Annu Rev Med* 64:407–425.

Supporting Information

Svidritskiy et al. 10.1073/pnas.1304922110

SI Materials and Methods

Preparation of *Escherichia coli* Ribosomes and Ribosomal Ligands. Salt-washed 70S ribosomes were prepared from MRE600 *E. coli* as described (1). $tRNA^{Met}$ and $tRNA^{Phe}$ were purchased from MP Biomedicals and Chemical Block, respectively. *N*-Ac-Phe-$tRNA^{Phe}$ and elongation factor G (EF-G) with 6-hisitidine tag were prepared and purified as previously described (2-4). $tRNA^{fMet}$ (Chemical Block) was aminoacylated using [^{35}S]-labeled methionine (Perkin Elmer) and formylated as described (5). Cy5-labeled protein S6 and Cy3-labeled protein L9 were incorporated into 30S and 50S subunits by partial reconstitution from 30S and 50S subunits carrying S6 and L9 deletions, respectively, as previously described (6). The ΔS6 strain of *E. coli* from the Keio Collection was purchased from the Genetic Stock Center (Yale University). Doubly labeled 70S ribosomes were isolated using previously described procedures (6).

Filter-Binding Assay. Before filter-binding experiments, 70S ribosomes were incubated with excess M0-27 mRNA (GGC AAG GAG GUA AAA *AUG UAA* AAA AAA, IDT) in the presence or absence of blasticidin S (BlaS; Fischer Scientific) in Buffer A [20 mM Tris·HCl (pH 7.5), 100 mM NH_4Cl, 20 mM $MgCl_2$, 5 mM β-mercaptoethanol]. The 70S complex was prepared at 400 nM and incubated at 37 °C for 30 min with 600 nM [^{35}S]-N-formyl-methionyl-$tRNA^{fMet}$ (fMet-$tRNA^{fMet}$). The fraction of ribosome-bound [^{35}S]-fMet-$tRNA^{fMet}$ was assayed by nitrocellulose filter (Whatman 0.45 μM) binding as described (7) and quantified using a scintillation counter. The relative occupancy of the P site by [^{35}S]-fMet-$tRNA^{fMet}$ in the presence of blasticidin S (Fig. 1) is expressed as the ratio of cpm of the complex in the presence of the antibiotic to cpm obtained for [^{35}S]-fMet-$tRNA^{fMet}$-bound ribosomes not treated with the antibiotic. Filter-binding experiments at each concentration of BlaS were performed three times.

RF1-Mediated Release Assay and Puromycin Reaction. *E. coli* 70S ribosomes and [^{35}S]-fMet-$tRNA^{fMet}$ were prepared as described above. *E. coli* release factor 1 (RF1) incorporating a C-terminal hexahistidine tag was overexpressed and purified as described (8, 9). A 30 nM pretermination complex was formed by incubating [^{35}S]-fMet-$tRNA^{fMet}$ with an equimolar amount of 70S ribosomes and a 200-fold excess of M0-27 mRNA (IDT), resulting in positioning of the UAA termination codon in the ribosomal A site. To estimate BlaS inhibition constants for [^{35}S]-fMet release by RF1 and for the puromycin reaction, the assays were carried out at subsaturating concentrations of RF1 (80 nM) and puromycin (50 μM), at which the observed rate constants were at least twofold lower than at saturating concentrations. For the peptide release assay, the pretermination complex was added to RF1 and incubated at room temperature in 20 mM Tris·acetate (pH 6.5), 100 mM ammonium acetate, 20 mM magnesium acetate, and 5 mM β-mercaptoethanol. Aliquots were removed from the reaction at 10 time points and quenched in six volumes of 0.1 N HCl. Hydrolyzed [^{35}S]-fMet was extracted with 0.7 mL of ethyl acetate, 0.6 mL of which was added to scintillation mixture and counted using a scintillation counter. All reactions were performed at pH 6.5, at which the [^{35}S]-fMet background signal is lower than that at pH 7.5, whereas reaction rates are not substantially affected. Puromycin reactions were carried out using a similar approach except that aliquots were quenched in 1 M CH_3COONa (pH 5.5) saturated with $MgSO_4$. Time progress curves for RF1-mediated release and puromycin reactions were obtained in the presence of 0, 30, 60, 100, 150, 300, 800, and 2,000 nM blasticidin S and 10,000 nM blasticidin S for the puromycin reactions. Catalytic rates (k_{obs}) estimated by a single-exponential fit for each concentration of BlaS were then fit to a hyperbola, yielding the apparent inhibition constant K_i. It is noteworthy that the experimental setup limits the determination of apparent K_i to 30 nM (pretermination complex concentration) and thus may underestimate the inhibitory effect of BlaS on the termination reaction (apparent K_i = 32 ± 18 nM). All experimental data were obtained by repeating experiments at least two times. Curve fitting of experimental data were performed using GraphPad Prism (GraphPad Software).

FRET Measurements and Data Analysis. Ribosomal complexes were assembled as previously described (10) in polyamine buffer containing 30 mM Hepes (pH 7.5), 6 mM $MgCl_2$, 6 mM β-mercaptoethanol, 150 mM NH_4Cl, 0.1 mM spermine, and 2 mM spermidine. Ribosomal complexes with single tRNA bound in the P site were assembled by incubating 70S S6-Cy5/L9-Cy3 ribosomes (300 nM) with mRNA m291 (600 nM) annealed to a biotinylated primer (800 nM), and $tRNA^{Met}$, $tRNA^{Phe}$, or $tRNA^{fMet}$ (600 nM) at 37 °C for 20 min. Pretranslocation ribosomal complexes were assembled by incubating ribosomal complexes with a single $tRNA^{Met}$ bound in the P site with *N*-Ac-Phe-$tRNA^{Phe}$ (450 nM) at 37 °C for 30 min. Complexes were diluted in polyamine buffer to ∼1 nM and immobilized on quartz slides. The buffer was exchanged with polyamine buffer described previously with the addition of an oxygen-scavenging mixture consisting of 0.8 mg/mL glucose oxidase, 0.625% glucose, ∼1.5 mM 6-hydroxy-2,5,7,8-tetramethylchromane-2-carboxylic (Trolox, triplet-state quencher), and 0.03 mg/mL catalase to slow the occurrence of photobleaching.

Single-molecule FRET (smFRET) measurements were taken as previously described (10), using an Olympus IX71 microscope with a UPlanApo 60×/1.20W objective. Cy3 and Cy5 dyes were excited using 532 nm and 642 nm lasers, respectively (Spectra-Physics); total internal reflection was achieved using a quartz prism (ESKMA Optics). A DV2 (Photometrics) dual-view imaging system equipped with a 630 nm dichroic mirror was used to split the fluorescence into Cy3 and Cy5 channels, which was recorded using an Andor iXon+ EMCCD camera through the program Single (downloaded from Taekjip Ha's laboratory website at the University of Illinois at Urbana–Champaign, physics.illinois.edu/cplc/software) with exposure time set to 100 ms. Imaging was carried out at room temperature.

smFRET movies were processed using IDL and analyzed in MATLAB using scripts freely available online at physics.illinois.edu/cplc/software. Apparent FRET efficiencies (E_{app}) were calculated from the donor (I_{Cy3}) and acceptor (I_{Cy5}) fluorescence intensities by $E_{app} = I_{Cy5}/[I_{Cy5}+I_{Cy3}]$. FRET distribution histograms were constructed from traces that showed single-step photobleaching events for both Cy5 and Cy3 using a Matlab script generously provided by Peter Cornish (University of Missouri, Columbia). Traces were normalized by length so that each trace contributes to a frequency count of 1. All histograms were smoothed with a five-point window and fit to the sum of two Gaussians. The peak positions were left unrestrained. The widths of the Gaussians were self-consistent and the residuals were random. Because less than 50% of the data for each set contained at least five transitions, data were not suitable for Hidden Markov modeling analysis (11, 12). The kinetic rates of transitions were determined by dividing the total number of transitions from one state to another by the total amount of time spent in the initial state.

Stopped-Flow Measurements of Presteady-State Translocation Kinetics. Kinetics of mRNA translocation was measured as previously described (12-15) with minor modifications. Pretranslocation complexes were constructed by incubation of 70S ribosomes (1 μM) with fluorescein-labeled mRNA (5′-GGC AAG GAG GUA AAA AUG UUU AAA-3′-fluorescein, synthesized by Dharmacon RNAi Technologies, 0.85 μM) and deacylated $tRNA^{Met}$ (2 μM) in polyamine buffer (20 mM Hepes·KOH, pH 7.5, 6 mM $MgCl_2$, 150 mM NH_4Cl, 6 mM β-mercaptoethanol, 2 mM spermidine, 0.1 mM spermine) for 20 min at 37 °C followed by incubation with *N*-acetyl-Phe-$tRNA^{Phe}$ (1.5 μM) for 30 min at 37 °C. Pretranslocation ribosomes were mixed with WT EF-G and GTP using an Applied Photophysics stopped-flow fluorometer. Final concentrations after mixing were: 35 nM ribosomes, 1.4 μM EF-G, and 0.5 mM GTP. Fluorescein was excited at 490 nm and fluorescence emission was detected using a 515 nm long-pass filter. Monochromator slits were adjusted to 9.3 nm. All stopped-flow experiments were done at 23 °C. Translocation of mRNA resulted in partial quenching of fluorescein coupled to the 3′ end of mRNA. Approximately 10 time traces were accumulated for each experiment. Time traces were analyzed using Pro-Data-Viewer software (Applied Photophysics). As has been reported previously (13–15), the kinetics of mRNA translocation are clearly biphasic and are best fitted by the sum of two exponentials, corresponding to apparent rate constants k_1 and k_2 (Table S2). Although the biphasic character of fluorescence changes associated with mRNA translocation is well documented (12), the physical basis of this phenomenon remains unclear. The rate of translocation was defined as the weighted average rate constant k_{av}, calculated as the sum of k_1 and k_2 normalized to their respective contributions to the total amplitude of fluorescence change [$k_{av} = (k_1{*}A_1 + k_2{*}A_2)/(A_1 + A_2)$] (12).

Crystal Structure Determination. 70S ribosomes were purified from wt *Thermus thermophilus* HB27 as described (8). A total of 4 μM ribosomes (final concentration) was incubated with twofold molar excess of $tRNA^{fMet}$ (Chemical Block), fivefold excess M0-27 mRNA (IDT), and 1 mM BlaS in buffer containing 25 mM Tris·acetate (pH 7.0), 50 mM potassium acetate, 10 mM ammonium acetate, and 10 mM magnesium acetate. Crystallization drops were formed by mixing 1.2 μL of the 70S·M027·$tRNA^{fMet}$·BlaS complex with 1.2 μL crystallization buffer [0.1 M Tris·HCl (pH 7.5), 4% (vol/vol) PEG 20000, 8% (vol/vol) 2-Methyl-2,4-pentanediol, and 0.2 M KSCN]. Crystallization was carried out by hanging-drop vapor diffusion using 0.5–0.8 M NaCl as reservoir solution. Cryoprotection was performed as described (9). Crystals were flash frozen by plunging into liquid nitrogen.

Crystals were screened at beam lines 23ID-B and 23ID-D at the Advanced Photon Source at Argonne National Laboratory and beam line X25 at the National Synchrotron Light Source at Brookhaven National Laboratory. Diffraction data were collected at beam line X25 at the NSLS using the PILATUS 6M PAD detector at an X-ray wavelength of 1.1 Å and an oscillation angle of 0.2°. For determining the structure of the 70S·M027·$tRNA^{fMet}$·BlaS complex, one dataset obtained from a single crystal was integrated and scaled using XDS. Two percent of the unique reflections were marked as test-set (R^{free} set) reflections and used for cross-validation throughout refinement. A previously determined X-ray structure of the 70S·RF2 termination complex obtained from the same crystal form (9) was used as a starting model for molecular replacement with tRNA, mRNA, and RF2 molecules removed. Density for tRNA, mRNA, and BlaS was clearly visible in initial F_{obs}-F_{calc} and $3F_{obs}$-$2F_{calc}$ difference maps. The BlaS molecule was built into difference density using the structural model from Protein Data Bank 1KC8 (16). Structure refinement was carried out using PHENIX (17) and CNS (18, 19) as described (9) and yielded a structure with R/R^{free} of 0.232/0.268 (Table S3). Superposition of 70S structures was performed by aligning 23S ribosomal RNA in PyMOL (20). Figures were rendered using PyMOL. The atomic coordinates and structure factors have been deposited in the Protein Data Bank (PDB ID codes 4L6J, 4L6K, 4L6L, and 4L6M).

1. Moazed D, Noller HF (1986) Transfer RNA shields specific nucleotides in 16S ribosomal RNA from attack by chemical probes. *Cell* 47(6):985–994.
2. Moazed D, Noller HF (1989) Intermediate states in the movement of transfer RNA in the ribosome. *Nature* 342(6246):142–148.
3. Wilson KS, Noller HF (1998) Mapping the position of translational elongation factor EF-G in the ribosome by directed hydroxyl radical probing. *Cell* 92(1):131–139.
4. Walker SE, Fredrick K (2008) Preparation and evaluation of acylated tRNAs. *Methods* 44(2):81–86.
5. Lancaster L, Noller HF (2005) Involvement of 16S rRNA nucleotides G1338 and A1339 in discrimination of initiator tRNA. *Mol Cell* 20(4):623–632.
6. Ermolenko DN, et al. (2007) Observation of intersubunit movement of the ribosome in solution using FRET. *J Mol Biol* 370(3):530–540.
7. Spiegel PC, Ermolenko DN, Noller HF (2007) Elongation factor G stabilizes the hybrid-state conformation of the 70S ribosome. *RNA* 13(9):1473–1482.
8. Laurberg M, et al. (2008) Structural basis for translation termination on the 70S ribosome. *Nature* 454(7206):852–857.
9. Korostelev A, et al. (2008) Crystal structure of a translation termination complex formed with release factor RF2. *Proc Natl Acad Sci USA* 105(50):19684–19689.
10. Cornish PV, Ermolenko DN, Noller HF, Ha T (2008) Spontaneous intersubunit rotation in single ribosomes. *Mol Cell* 30(5):578–588.
11. Studer SM, Feinberg JS, Joseph S (2003) Rapid kinetic analysis of EF-G-dependent mRNA translocation in the ribosome. *J Mol Biol* 327(2):369–381.
12. Ermolenko DN, Noller HF (2011) mRNA translocation occurs during the second step of ribosomal intersubunit rotation. *Nat Struct Mol Biol* 18(4):457–462.
13. Munro JB, et al. (2010) Spontaneous formation of the unlocked state of the ribosome is a multistep process. *Proc Natl Acad Sci USA* 107(2):709–714.
14. Peske F, Savelsbergh A, Katunin VI, Rodnina MV, Wintermeyer W (2004) Conformational changes of the small ribosomal subunit during elongation factor G-dependent tRNA-mRNA translocation. *J Mol Biol* 343(5):1183–1194.
15. Shi X, Chiu K, Ghosh S, Joseph S (2009) Bases in 16S rRNA important for subunit association, tRNA binding, and translocation. *Biochemistry* 48(29):6772–6782.
16. Hansen JL, Moore PB, Steitz TA (2003) Structures of five antibiotics bound at the peptidyl transferase center of the large ribosomal subunit. *J Mol Biol* 330(5):1061–1075.
17. Adams PD, et al. (2002) PHENIX: Building new software for automated crystallographic structure determination. *Acta Crystallogr D Biol Crystallogr* 58(Pt 11):1948–1954.
18. Brünger AT, et al. (1998) Crystallography & NMR system: A new software suite for macromolecular structure determination. *Acta Crystallogr D Biol Crystallogr* 54(Pt 5):905–921.
19. Brünger AT, Adams PD, Rice LM (1997) New applications of simulated annealing in X-ray crystallography and solution NMR. *Structure* 5(3):325–336.
20. DeLano, WL (2002) The PyMOL Molecular Graphics System (DeLano Scientific, Palo Alto, CA).

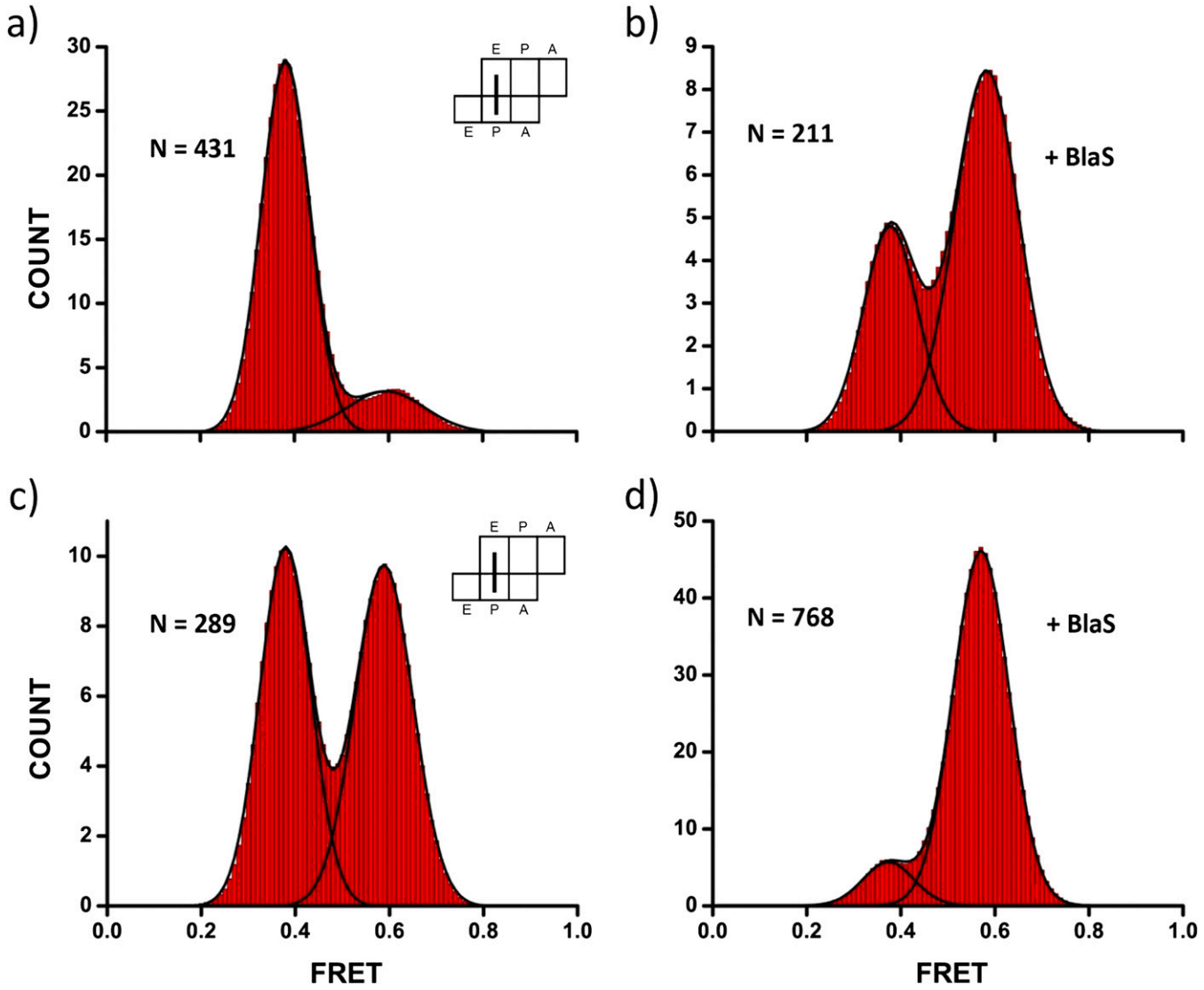

Fig. S1. BlaS inhibits counterclockwise rotation of the 30S subunit coupled to the movement of deacylated $tRNA^{Met}$ or $tRNA^{fMet}$ into the hybrid P/E state. Histograms showing distributions of FRET values in ribosomes containing deacylated $tRNA^{Met}$ (*A* and *B*) or deacylated $tRNA^{fMet}$ (*C* and *D*) in the P site in the absence (*A* and *C*) or presence of BlaS (*B* and *D*). N, number of single-molecule FRET traces compiled.

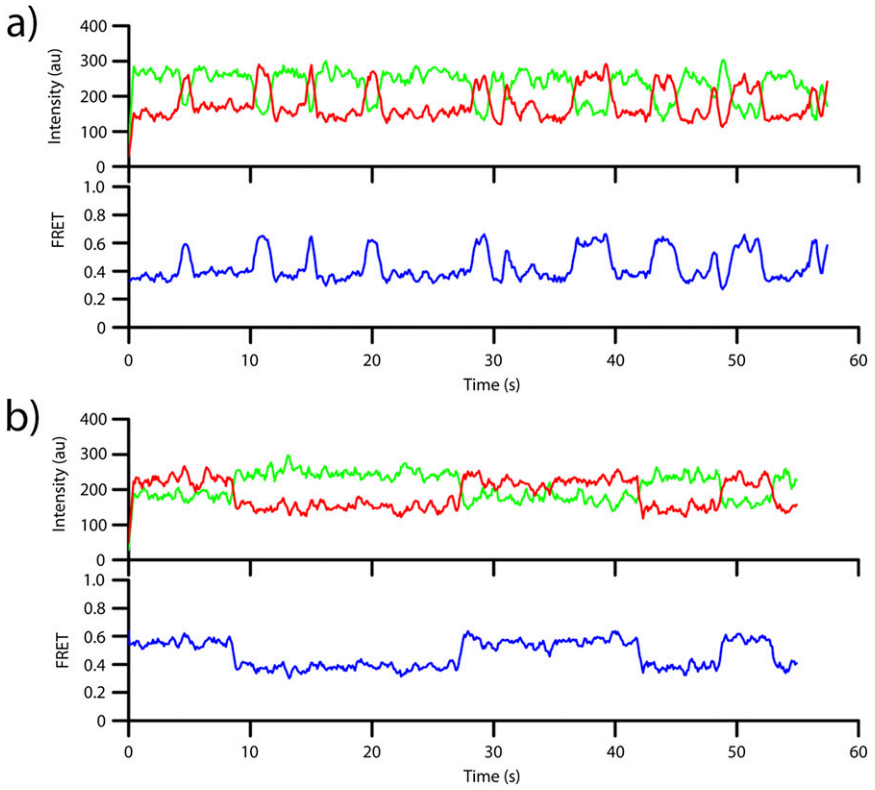

Fig. S2. Representative time traces of 70S ribosomes containing S6-Cy5 and L9-Cy3 with $tRNA^{Met}$ in the P site and *N*-Ac-Phe-$tRNA^{Phe}$ in the A site imaged in the absence (*A*) or presence (*B*) of BlaS. Cy3 and Cy5 fluorescence intensities are represented by green and red traces, respectively. Calculated FRET is shown as the blue trace.

Table S1. Proportions of rotated and nonrotated ribosomes and rates of spontaneous rotation in the presence and absence of BlaS derived from smFRET

70S complex	Percent NR	Percent R	$k_{0.6\rightarrow0.4}$, s^{-1}	$k_{0.4\rightarrow0.6}$, s^{-1}	K_{eq} (rates)	K_{eq}, %R/%NR	Percent trans
Deacylated tRNA in P site							
$tRNA^{Phe}$	32	68	0.87	0.23	3.8	2.1	51
$tRNA^{Phe}$ with BlaS	78	22	0.19	0.28	0.7	0.3	24
$tRNA^{Met}$	15	85	0.62	0.17	3.7	5.7	34
$tRNA^{Met}$ with BlaS	67	33	0.14	0.14	1.0	0.5	43
Pretranslocation complexes							
$tRNA^{Met}$/*N*-Ac-Phe-$tRNA^{Phe}$	28	72	0.90	0.29	3.1	2.6	33
$tRNA^{Met}$/*N*-Ac-Phe-$tRNA^{Phe}$ with BlaS	41	59	0.14	0.07	2.0	1.4	37

Percent of pretranslocation ribosomes in nonrotated (NR), 0.6 FRET state or rotated (R), 0.4 FRET state derived from FRET distribution histograms (Figs. 2 and 3). SD was 5%. Rates of counterclockwise ($k_{0.6\rightarrow0.4}$) and clockwise ($k_{0.4\rightarrow0.6}$) intersubunit rotation are calculated as number of transitions/dwell time. Equilibrium constants (K_{eq}) were calculated from the ratio of rates for forward and reverse rotation. These values deviate somewhat from equilibrium constants calculated from the relative populations of rotated and nonrotated ribosomes (K_{eq}, %R/%NR) because of the presence of a fraction of ribosomes that do not display fluctuations in smFRET time traces and thus skew equilibrium constant values derived from the distribution histogram. The percentage of traces with fluctuations (percent trans) is defined as the total number of traces that contain at least one FRET transition between 0.6 and 0.4 FRET states divided by the total number of traces.

Table S2. Rates of EF-G-mediated mRNA translocation in the absence and presence of BlaS

	k_1, s^{-1}	k_2, s^{-1}	$A_1/(A_1+A_2)$	k_{av}, s^{-1}
EF-G-GTP	6.0 ± 0.9	0.5 ± 0.1	0.56 ± 0.05	3.7 ± 0.6
EF-G-GTP + 1 mM BlaS	5.2 ± 0.7	0.4 ± 0.1	0.46 ± 0.01	2.6 ± 0.4

Kinetics of mRNA translocation was measured in presteady-state stopped-flow kinetic experiments by quenching of fluorescein attached to the mRNA (Fig. 3C). k_1 and k_2 are the rate constants of double-exponential fits of the mRNA translocation data; $A_1/(A_1+A_2)$ is the relative contribution of the faster phase to the total amplitude of fluorescein quenching. Weighted average values (k_{av}) for mRNA translocation rates were calculated by combining the rate constants derived from the double-exponential fits: $k_{av} = (k_1A_1 + k_2A_2)/(A_1 + A_2)$. The rates of both the fast (k_1) and slow (k_2) phases of translocation were not significantly affected by BlaS. However, in the presence of BlaS, the amplitude of the slow phase increased at the expense of the fast phase, resulting in a small decrease in k_{av}.

Table S3. Data collection and refinement statistics

	Statistics
Data collection	
Space group	$P2_12_12_1$
Cell dimensions	
a, *b*, *c*; Å	211.53, 454.44, 620.87
α, β, γ; °	90, 90, 90
Resolution, Å	70-3.4 (3.4–3.53)*
$R_{p.i.m.}$[†]	0.158 (0.88)
CC(1/2)[‡]	99.3 (37)
I/σ*I*	7.44 (1.01)[§]
Completeness, %	100 (100)
Redundancy	9.9 (10)
Refinement	
Resolution, Å	50–3.4
No. reflections	810,608
R^{work}/R^{free}	0.232/0.268
No. atoms	293,128
Ions modeled as Mg^{2+}	4,363
rmsd	
Bond lengths, Å	0.003
Bond angles, °	0.618

*Values in parentheses are for the high-resolution shell.
[†]$R_{p.i.m.}$, precision-indicating merging R factor (1) was calculated using SCALA (2).
[‡]CC(1/2) is the percentage of correlation between intensities from random half-datasets as defined by Karplus and Diederichs (3).
[§]I/σI = 2.0 at 3.65 Å.

1. Weiss MS (2001) Global indicators of X-ray data quality. *J Appl Cryst* 34(2):130–135.
2. Collaborative Computational Project, Number 4 (1994) The CCP4 suite: programs Programs for protein crystallography. *Acta Crystallogr D Biol Crystallogr* 50(Pt 5):760–763.
3. Karplus PA, Diederichs K (2012) Linking crystallographic model and data quality. *Science* 336(6084):1030–1033.